



## Platelet-like Particles Dynamically Stiffen Fibrin Matrices and Improve Wound Healing Outcomes

Journal:	<i>Biomaterials Science</i>
Manuscript ID	BM-ART-09-2018-001201.R1
Article Type:	Paper
Date Submitted by the Author:	14-Dec-2018
Complete List of Authors:	Nandi, Seema; North Carolina State University College of Engineering, Biomedical Engineering Sproul, Erin; North Carolina State University College of Engineering, Biomedical Engineering Nellenbach, Kimberly; North Carolina State University College of Engineering, Biomedical Engineering Erb, Mary; North Carolina State University College of Engineering, Biomedical Engineering Gaffney, Lewis; North Carolina State University College of Engineering, Biomedical Engineering Freytes, Donald; North Carolina State University College of Engineering, Biomedical Engineering Brown, Ashley; North Carolina State University College of Engineering, Biomedical Engineering

# Platelet-like Particles Dynamically Stiffen Fibrin Matrices and Improve Wound Healing Outcomes

*Seema Nandi<sup>1,2</sup>, Erin P. Sproul<sup>1,2</sup>, Kimberly Nellenbach<sup>1,2</sup>, Mary Erb<sup>1</sup>, Lewis Gaffney<sup>1,2</sup>, Donald O. Freytes<sup>1,2</sup>, and Ashley C. Brown<sup>1,2</sup>*

## **Authorship**

Contribution: S.N., E.P.S., K.N., M.E., and L.G. performed experiments; S.N., E.P.S., M.E. and A.C.B. analyzed results; S.N., L.G., and A.C.B. made figures; S.N., D.O.F., and A.C.B. designed the research; S.N. and A.C.B. wrote the paper.

Correspondence: Ashley C. Brown, Advanced Wound Healing Laboratory, Joint Department of Biomedical Engineering, North Carolina State University and The University of North Carolina at Chapel Hill, Raleigh, NC 27607; email: [aecarso2@ncsu.edu](mailto:aecarso2@ncsu.edu).

## **Abstract**

Native platelets perform several critical functions within the context of wound healing, including participating in initial hemostasis and interacting with fibrin at the wound site to induce clot retraction. Platelet depletion or dysfunction due to trauma or disease can inhibit robust wound healing responses. There has been a focus recently on developing synthetic, non-immunogenic platelet mimetic technologies for the purpose of augmenting hemostatic responses in cases of deficient native platelet functionality. Here we describe the application of synthetic platelet-like particles (PLPs), capable of recapitulating the deformable platelet body and fibrin specificity found in native platelets, to enhance healing outcomes. We first demonstrate PLPs mimic activated platelet morphology and induce fibrin clot retraction. During clot retraction, native platelets generate forces within a fibrin network to stiffen the fibrin matrix; therefore, we

<sup>1</sup>Joint Department of Biomedical Engineering, North Carolina State University and The University of North Carolina at Chapel Hill, Raleigh, NC 27695

<sup>2</sup>Comparative Medicine Institute, North Carolina State University, Raleigh, NC 27695

hypothesized that our PLPs will likewise be able to stiffen provisional fibrin matrices. Due to previous studies indicating that increased matrix stiffness is linked to increased cellular migration, we further hypothesize that PLP-mediated fibrin stiffening will enhance cell migration and improve healing outcomes within *in vitro* and *in vivo* models of wound healing. PLPs were found to enhance fibroblast migration in *in vitro* models of early wound healing and enhance healing outcomes in an *in vivo* murine model of wound healing. These studies demonstrate the utility of PLPs for enhancing wound repair and also provide insight into the role of native platelet-mediated clot retraction in wound healing.

## **Introduction**

Native platelets play a multitude of functions in the wound healing process, including binding to fibrin fibers formed at a wound site, catalyzing clot formation to bring about hemostasis, and exerting strain upon these fibers to induce clot retraction. During the coagulation process, platelets become activated in response to injured vasculature and thrombin generation, allowing them to specifically target injury sites and interact with fibrin to form a platelet-fibrin “plug” to stabilize initial bleeding.<sup>1,2</sup> Platelets then exert strain upon fibrin fibers within the clot network via actin- and myosin-driven contraction, causing microcollapses in the fibrin network that build to generate a bulk clot retraction event.<sup>3</sup> Clot retraction stabilizes the clot and decreases its surface area to allow blood perfusion to healing tissues;<sup>4,5</sup> additionally, clot retraction results in the expulsion of serum from the clot and brings about an overall stiffening of the fibrin clot, creating a provisional fibrin matrix capable of supporting infiltration by inflammatory cells and fibroblasts.<sup>3-5</sup> After clot retraction, inflammatory cells, fibroblasts, and keratinocytes migrate throughout the wound site to prevent infection and begin the process of tissue repair and remodeling. Fibroblasts and keratinocytes migrate within the matrix, respectively synthesizing

and depositing new collagen or differentiating to reform the epidermis.<sup>6</sup> Matrix stiffness has been shown to affect cellular behaviors, including cellular migration and proliferation;<sup>7,8</sup> therefore, we hypothesize that platelet-mediated stiffening of the provisional fibrin matrix that comes about as a result of clot contraction promotes subsequent stages of wound healing, including cell migration and proliferation within the wound bed and tissue repair.

Traumatic injury and/or disease can cause platelet depletion or dysfunction, inhibiting the clot retraction event and thus preventing clot stiffening and stabilization and inhibiting perfusion of blood to healing tissues.<sup>9-12</sup> Platelet depletion can inhibit effective platelet participation in primary and secondary hemostasis, preventing formation of a robust platelet “plug” and inhibiting formation of a stable clot. This depletion can occur as a result of uncontrolled bleeding after traumatic injury or as a result of disease, including as a side effect of HIV or chemotherapy. Platelet dysfunction can also occur as a result of disease; a notable example of this manifests in the lack of robust clotting experienced by those suffering from Von Willebrand disease. Current clinical treatments for platelet depletion or dysfunction generally focus on using natural platelet replacement technologies, including platelet transfusions and lyophilized platelets, to augment native platelet activity and treat impaired healing. However, these technologies are limited by high costs, short shelf life, and potential immunogenicity; therefore, recent studies have focused on the development of synthetic platelet mimetic technologies for the purpose of augmenting hemostasis while minimizing potential adverse immune responses.<sup>1, 13, 14</sup> Our lab has previously described the formation and characterization of synthetic platelet-like particles (PLPs) capable of recapitulating key mechanical and biological functions of native platelets, i.e. binding specifically to fibrin and deforming to mechanically induce clot retraction, by covalently coupling highly deformable ultralow crosslinked (ULC) poly(*N*-isopropylacrylamide) (pNIPAm)

microgels to a fibrin-specific single domain variable fragment (sdFv).<sup>15</sup> Like native activated platelets, these particles are capable of a high degree of deformability, as indicated by atomic force microscopy (AFM) characterization of ULC deformation on a glass surface.<sup>16</sup> Natural platelets have been shown to generate forces within fibrin matrices, resulting in clot contraction and matrix stiffening;<sup>3, 4</sup> however, the ability of PLPs to recapitulate this active force generation within fibrin matrices to generate bulk clot stiffening is not yet known. The effect of any potential PLP-induced clot stiffening upon fibroblast migration *in vitro* and corresponding healing *in vivo* has also not previously been investigated. In this study, we investigate the ability of these PLPs to promote fibroblast migration and enhance wound healing outcomes. We first characterize PLPs formed by covalently coupling these highly deformable ULC microgels to a fibrin-specific fragment E antibody and then apply these PLPs to fibrin networks *in vitro* and *in vivo* to mechanically enhance wound healing outcomes. We hypothesize that, due to their platelet-like highly deformable ULC body and high fibrin specificity, these PLPs will be able to recapitulate platelet-like induction of microcollapses within and subsequent contraction of fibrin clots, resulting in increased matrix stiffness and subsequently enhancing both fibroblast migration throughout the provisional fibrin matrix *in vitro* and wound healing outcomes *in vivo*. These studies demonstrate the utility of PLPs for enhancing wound repair and also provide insight into the role of native platelet-mediated clot retraction in wound healing.

## **Materials and Methods**

### *Microgel Synthesis and Characterization*

Ultralow crosslinked (ULC) poly(*N*-isopropylacrylamide-*co*-acrylic acid) (pNIPAm) microgels were synthesized via a precipitation polymerization reaction. NIPAm (Sigma-Aldrich, St. Louis, MO, USA) was recrystallized in hexanes prior to use. NIPAm and acrylic acid (Sigma-Aldrich,

St. Louis, MO, USA) were dissolved in ultrapure water at a concentration of 140 mM total monomer (10% acrylic acid, 90% NIPAm). Acrylic acid was incorporated into the solution to provide functional groups on the ULC surface for coupling of fibrin-binding antibodies. The solution was filtered through a 0.2  $\mu\text{m}$  pore filter and added into a 500 mL 3-neck round-bottom flask. A silicon oil bath was heated to 70  $^{\circ}\text{C}$ , and then the 3-neck flask containing the monomer solution was added into the bath and equilibrated at 70  $^{\circ}\text{C}$  for one hour under constant stirring at 450 rpm. During equilibration, the solution was purged with nitrogen. After the equilibration period, the reaction was initiated using 22.8 mg ammonium persulfate (APS) (Sigma-Aldrich, St. Louis, MO, USA) dissolved in 1 mL ultrapure water for a final concentration of 1 mM APS. The reaction was carried out for 6 hours at constant temperature and stir speed of 70  $^{\circ}\text{C}$  and 450 rpm. The solution turned opaque following addition of APS, indicating polymer formation. After 6 hours, the reaction was cooled overnight while maintaining constant stirring at 450 rpm. The microgel solution was then filtered through glass wool and dialyzed (MWCO: 1000kD from Spectrum Labs, Rancho Dominguez, CA, USA) against ultrapure water for 3 days for purification. Purified microgels were lyophilized and resuspended in ultrapure water.

ULC size was characterized in 10 mM formate buffer (pH 3.0) using a Malvern NanoSight NS300 (Malvern Instruments, Worcestershire, UK) to determine particle hydrodynamic radii and size distribution. Size and distribution was determined from 5 measurements of 30 seconds each. ULCs were also measured in 10 mM HEPES buffer (pH 7.4) using a Malvern Zetasizer Nano S to perform dynamic light scattering (DLS) to evaluate ULC hydrodynamic radii under physiological pH. ULC deformability on a glass surface was characterized using an Asylum Research MFP-3D Bio atomic force microscope (Asylum Research, Santa Barbara, CA, USA).<sup>17, 18</sup> Glass coverslips were cleaned via submersion in a

series of solutions (alconox, water, acetone, absolute ethanol, and isopropyl alcohol) in an ultrasonic bath. ULCs were deposited onto dry coverslips, allowed to dry overnight, and characterized using silicon nitride cantilevers ( $k = 42 \text{ N ml}$ , NanoWorld) operated in intermittent contact mode. Average ULC diameter, height, and spread areas were determined from a minimum of 30 particles using ImageJ image analysis software (National Institutes of Health, Bethesda, MD, USA).

ULC morphology was characterized using a JEOL 7600F cryogenic scanning electron microscope (cryoSEM) with a Gatan Alto Cryo-transfer system. ULC samples suspended in ultrapure water were plunge-frozen in liquid nitrogen under high pressure, fractured and etched for five minutes under vacuum, gold sputter-coated, and imaged. ULC morphology was compared to native active platelet morphology. To isolate platelets for cryoSEM, platelet-rich plasma was first isolated from blood acquired from the New York Blood Center (New York, NY, USA) by centrifugation at  $150 \times g$  for 15 minutes with no deceleration. Platelet-rich plasma was then centrifuged at  $900 \times g$  for 5 minutes to isolate platelets.<sup>19</sup> Platelets were washed and resuspended in Tyrode's albumin buffer and activated with  $0.25 \text{ U/ml}$  human  $\alpha$ -thrombin (Enzyme Research Laboratories, South Bend, IN, USA), then imaged immediately following activation.

#### *PLP Synthesis and Characterization*

Platelet-like particles (PLPs) were created by covalently coupling ULCs to a sheep anti-human fibrin fragment E polyclonal IgG antibody (Affinity Biologicals, Ancaster, ON, CAN) using EDC/NHS chemistry.  $3.625 \times 10^{-2} \text{ mg}$  ULCs were suspended in ultrapure water at a concentration of  $0.5 \text{ mg/ml}$ . ULCs were incubated with  $500 \text{ uL}$  of  $50 \text{ mg/ml}$  EDC in ultrapure water and  $500 \text{ uL}$  of  $5 \text{ mg/ml}$  sulfo-NHS in ultrapure water for 30 minutes. Following EDC/NHS

incubation, HEPES buffer (10 mM, pH 7.4) and 10 mg of antibody were added to obtain a 2:1 ratio of antibody to AAc present in the ULCs. The reaction was allowed to proceed for 4 hours and then PLPs were purified via dialysis against ultrapure water with 3 buffer changes over 24 hours at 4°C. Purified PLPs were then lyophilized and resuspended in ultrapure water at desired concentrations for subsequent experiments.

#### *Determination of fibrin clot structure in the presence of PLPs*

PLP impact on fibrin clot structure was determined via confocal microscopy using a Zeiss Laser Scanning Microscope (LSM 710, Zeiss Inc., Jena, GER) at a magnification of 63X. Control fibrin clots were comprised of 2 mg/ml human fibrinogen (FIB 3, Enzyme Research Laboratories, South Bend, IN, USA) and 0.1 U/ml human  $\alpha$ -thrombin (Enzyme Research Laboratories, South Bend, IN, USA). Fibrin + ULC (0.5 mg/mL) clots and fibrin + PLP (0.5 mg/mL) clots were also imaged to determine differences in clot microstructure in the presence of unconjugated (non-binding) ULCs and in the presence of conjugated (fibrin-binding) PLPs. All samples were imaged 24 hours after polymerization. Alexa-fluor 488 labeled fibrinogen was utilized for visualization in all clots, and clots were formed between a glass slide and a coverslip and prior to imaging. Three clots were imaged per group, and three random 5.06  $\mu$ m z-stacks were imaged per clot. Z-stacks were imported into ImageJ and made binary so that fibrin fibers appeared black and negative space appeared white. Clot density was assessed by calculating the area of black pixels divided by the area of white pixels in each image.

Clot structure was additionally assessed via cryoSEM. Control fibrin clots composed of 2 mg/ml human fibrinogen (FIB 3, Enzyme Research Laboratories, South Bend, IN, USA) and 0.1 U/ml human  $\alpha$ -thrombin were imaged 24 hours after polymerization. Fibrin clots

incorporated with 0.5 mg/ml PLPs or 0.5 mg/ml ULCs were also imaged. Three clots were imaged per group, and three random images were taken per clot.

#### *Characterization of forces generated by PLPs within a fibrin network*

Forces generated by PLPs within a fibrin network were quantified by modifying an established micropost deflection technique.<sup>20-25</sup> Dow Corning Sylgard 184 polydimethylsiloxane (PDMS) (Krayden, Denver, CO, USA) microposts spaced 2 mm apart from one post center to the opposing post center (**Figure S1a**) were seeded with standard fibrin clots, fibrin + PLP clots, or fibrin + ULC clots according to clot compositions imaged via cryoSEM. Forces generated within the fibrin clot networks caused deflection of the PDMS microposts. We then quantified forces generated within the clots from the deflection distance of the microposts using a linear elastic model based on the micropost geometry and elastic modulus using Hooke's law:

$$F = k\delta$$

in which  $F$  represents the force ( $\mu\text{N}$ ) applied to cause the micropost deflection,  $\delta$  represents the deflection distance ( $\mu\text{m}$ ), and  $k$  represents the spring constant of the microposts. The spring constant  $k$  was determined using a linear elastic model based on the micropost geometry and the PDMS elastic modulus:

$$k = \frac{3\pi ED^4}{64L^3}$$

where  $E$  is the elastic modulus of the PDMS used to create the microposts and  $D$  and  $L$  are the diameter ( $200 \mu\text{m}$ ) and length ( $1 \text{ mm}$ ) of the microposts, respectively. The spring constant  $k$  was determined to be  $7.5 \text{ N/m}$ , giving a force vs. displacement curve (**Figure S1b**) modeled by the equation

$$F = 7.5\delta$$

Post displacement was determined using ImageJ image analysis software (National Institutes of Health, Bethesda, MD, USA). The design of the microposts allowed for up to 16 independent sets of micropost deflection measurements to be taken per well; each individual set of microposts was seeded with one clot, allowing for up to 16 independent clot contraction events within each well. In practice, for each experiment, only 5-6 posts were seeded within one well to ensure that all posts could be seeded and imaged in a timely manner. For quantification, measurements were then taken from the center of one post to the center of the opposite post. Post centers were determined based on the known post geometry, using the known post diameter to determine the center of each post. Post deflection distances were measured blinded so as to reduce the risk of introducing bias into the observed measurements. Three independent experiments were conducted, with a minimum of 5 samples per group per experiment.

#### *Characterization of fibrin network stiffness in the presence of PLPs*

Fibrin network stiffness was evaluated with an atomic force microscope (AFM) (Asylum MFP-3D, Asylum Research, Santa Barbara, CA, USA) in contact force mode using silicon nitride cantilevers (Nanoandmore, Watsonville, CA, USA). Cantilevers had a particle diameter of 14.45  $\mu\text{m}$  to ensure that the cantilever would be larger than individual pores within the fibrin matrix. The spring constant of each cantilever was determined using the AFM software (Igor Pro 15). 10  $\mu\text{m}$  x 10  $\mu\text{m}$  force maps were collected for control fibrin clots, fibrin + PLP clots, and fibrin + ULC clots at concentrations corresponding to the clots used for confocal microscopy, cryoSEM, and post deflection studies. Each force map was fitted by applying the Hertz model, which is commonly used for biological samples, to the linear region of the force curve to obtain the Young's modulus of the clot, as done in similar works.<sup>26</sup> The model was fitted to the linear region of the curve because the Hertz model assumes that a measured sample is isotropic and

linear elastic. It also assumes that the indenter (cantilever tip) is not deformable and that the indentation into the sample is negligible in comparison to sample thickness. The calculations of the Young's modulus are based on assumptions regarding the cantilever tip geometry, tip material, and Poisson ratio value of the sample.<sup>27, 28</sup> In order to apply the Hertz model to the clots measured in this study, we formed clots approximately 1 cm in thickness and assumed a silicon nitride tip and a spherical tip geometry with a radius of 990 nm. The Poisson's ratio was set to 0.33. Clots were allowed to polymerize for 1 hour; measurements were taken immediately following fibrin network polymerization and again 24 hours after polymerization. A minimum of three clots were analyzed per group, with at least three force maps of 256 force curves each taken per clot. The average Young's modulus  $\pm$  standard deviation was reported for each group.

#### *Evaluation of PLP-mediated cell migration in vitro*

Neonatal human dermal fibroblasts (HDFn) (Gibco, Waltham, MA, USA) (P5-P13) were cultured into three-dimensional spheroids over 72 hours using a hanging drop cell culture technique.<sup>29</sup> Fibrin networks composed of 2 mg/ml human fibrinogen (FIB 3, Enzyme Research Laboratories, South Bend, IN, USA) and 0.1 U/ml human  $\alpha$ -thrombin (Enzyme Research Laboratories, South Bend, IN, USA) were created in the wells of a 48-well tissue culture plate (VWR, Radnor, PA, USA). After polymerization of the fibrin clot layer for one hour, spheroids were transferred onto the fibrin clot layer using a 21 G x 1 1/2' needle (BD Biosciences, San Jose, CA, USA) and then covered with a second fibrin layer. Spheroids were also embedded in fibrin networks that contained 0.5 mg/ml PLPs, 1.0 mg/ml PLPs, or 0.5 mg/ml unconjugated ULCs. After polymerization of the second layer, HDFn growth medium (DMEM, 10% fetal bovine serum, 1% penicillin-streptomycin, 1% L-glutamine) was added into each well, and spheroids were imaged every 24 hours for a 72-hour period; cell migration throughout the matrix was

quantified by measuring area of the spheroid using ImageJ image analysis software. Fibroblast migration through fibrin networks comprised of 4 mg/ml fibrinogen in the presence or absence of PLPs (0.5 mg/ml) was also evaluated in order to determine the effects of PLPs on migration at both the upper and lower boundaries (2-4 mg/ml) of physiological fibrinogen concentrations.<sup>30-32</sup> Migration through networks comprised of 2 mg/ml fibrinogen in the presence of uncharged ULCs (0.5 mg/ml) was also evaluated to determine the influence of ULC charge on migration. Six samples were analyzed per group.

#### *Evaluation of PLP-mediated wound closure in vivo*

Wound healing *in vivo* in the presence of PLPs was assessed using a murine wound healing model previously described by Dunn *et al.*<sup>33</sup> 8 week old C57/B6 mice (Charles River Laboratories, Wilmington, MA, USA) were anesthetized through a nose cone for the duration of surgery using general anesthesia (5% isoflurane in oxygen at a flow rate of 2 L/min, maintained at 2-3% isoflurane). Full thickness dermal wounds extending through the panniculus carnosus were excised using 4 mm biopsy punches (Fisher Scientific, Hampton, NH, USA). Wounds were splinted with 10 mm silicone rings with a 5 mm inner diameter for the ring openings. This was done in order to ensure healing via re-epithelialization rather than skin contraction so as to model human wound healing. 10  $\mu$ L PLP treatments were applied topically at concentrations of 0, 0.5, 1.0, or 2.0 mg/ml PLPs in 0.9% sterile filtered saline (n = 5 wounds/group). Wounds were imaged and then covered with waterproof, but water vapor permeable, Opsite bandages (Fisher Scientific, Hampton, NH, USA). For post-operative pain relief, carprofen (5 mg/kg) was administered subcutaneously prior to removal of mice from anesthesia. Wounds were imaged and Opsite dressings were changed every day for nine days post-injury. Carprofen was administered once daily for the first five days post-injury. Wound size analysis was performed

on daily wound images that were blinded by treatment group and randomized using a random number generator. Wound boundaries were determined manually through apparent differences in tissue texture and color between wounded and healed areas. Wound sizes were quantified using ImageJ image analysis software and normalized to the standardized silicone ring openings, and the normalized areas were used to determine closure rates for wounds in each treatment group.

Dermal tissue surrounding the wounds was excised nine days post-surgery and fixed in 10% formalin. Samples were then dehydrated, embedded in paraffin, and sectioned for histological and immunohistochemical analysis. Martius Scarlet Blue (MSB) staining was performed to identify collagen and fibrin within the wound site. Epidermal thickness was quantified from MSB images by measuring the thickness of the epidermal layer at 4 regions evenly spaced across the wound area for 5 samples per group. CD31 labeling was also performed in order to evaluate angiogenesis within tissue forming at the wound sites. For immunohistochemistry, tissue was deparaffinized, rehydrated, and incubated with 1% goat serum (Thermo Fisher Scientific, Waltham, MA, USA). Sections were labeled with monoclonal antibody to CD31 (1:50, clone SP38, Thermo Fisher Scientific, Waltham, MA, USA) overnight at 4 °C. Sections were then washed in PBS and labeled with a secondary antibody (Alexa 594) for one hour at room temperature. Following incubation with the secondary antibody, sections were washed in PBS and mounted with Vectashield HardSet mounting medium with DAPI (Fisher Scientific, Hampton, NH, USA). CD31 positively labeled tissue was quantified by ImageJ using Particle Analysis to measure total red area (defined as red area greater than  $1.0 \mu\text{m}^2$  with a threshold of 0-50) for 5 wounds per treatment condition. In order to assess PLP incorporation throughout the wound tissue, sections were labeled with a monoclonal antibody to fibrin (1:66.7, clone UC45, GeneTex, Irvine, CA, USA) overnight at 4 °C. Sections were then

washed in PBS and labeled with a monoclonal antibody (Alexa 594) to label fibrin and a polyclonal anti-sheep 488 FITC-conjugated antibody to label the sheep anti-human antibody present on the PLPs. Following incubation with the secondary antibody, sections were washed with PBS and mounted with Vectashield HardSet mounting medium with DAPI (Fisher Scientific, Hampton, NH, USA).

An additional *in vivo* study was performed to evaluate the ability of PLPs to enhance wound healing when incorporated into a fibrin polymer and to compare PLP-induced healing with a standard-of-care technology. Using the full thickness dermal injury model described above, mice were treated with saline, fibrin polymers, fibrin + ULC polymers, fibrin + PLP polymers, or platelet-rich plasma (PRP), which is currently used clinically as a standard-of-care in wound healing treatments (n = 5 wounds/group).<sup>34-36</sup> To obtain PRP, blood was collected from 8 week old C57/B6 mice via cardiac puncture and then centrifuged at 150 x g for 15 minutes to isolate PRP. All fibrin polymers were composed of 2 mg/ml human fibrinogen (FIB 3, Enzyme Research Laboratories, South Bend, IN, USA) and 0.1 U/ml human  $\alpha$ -thrombin (Enzyme Research Laboratories, South Bend, IN, USA). Fibrin + ULC polymers and fibrin + PLP polymers contained 0.5 mg/ml ULCs or PLPs, respectively; this concentration was chosen because 0.5 mg/ml PLPs was determined as the optimal concentration for improving fibroblast migration responses within a fibrin + PLP polymer in the *in vitro* spheroid migration assays described above. Dermal tissue surrounding the wounds were excised 9 days post-surgery and processed for histological and immunohistochemical analysis as described above. Mean  $\pm$  standard deviation is presented for all quantitative analysis of healing parameters. All procedures were approved by the North Carolina State University IACUC and were performed under the approved protocol number 16-228-B.

### *Statistical analysis*

Statistical analysis was performed in GraphPad Prism 7 (GraphPad, San Diego, CA, USA). Data was analyzed via a one-way analysis of variance (ANOVA) with a Tukey's post hoc test using a 95% confidence interval for all measurements. Outlier tests were performed on all datasets prior to graph creation and statistical analysis.

## **Results and Discussion**

### *ULC microgels mimic the morphology of activated platelets*

ULC microgels were synthesized via precipitation polymerization techniques (**Figure 1a**). ULC microgels were previously shown to be highly deformable and capable of changing shape, as marked by ULC deformability on a glass surface visualized via atomic force microscopy (AFM).<sup>15</sup> We hypothesized that this shape change would allow ULCs to mimic the spindle-like morphology of activated platelets; therefore, we characterized the size, deformability, and morphology of our ULCs in order to verify their ability to take on morphologies and mechanically deform in a manner reminiscent of native platelets. Size and distribution of ULCs were characterized using nanoparticle tracking analysis with a Malvern Nanosight NS300. ULCs were suspended in 10 mM formate buffer (pH 3.0) in order to obtain particle hydrodynamic radii and size distribution in a collapsed conformation. ULCs were found to have hydrodynamic radii of  $624 \pm 32$  nm, with a Gaussian size distribution (**Figure 1b**). ULCs were also characterized in 10 mM HEPES buffer (pH 7.4). At physiological pH, ULCs were found to have an average hydrodynamic radius of  $1.56 \mu\text{m} \pm 97.4$  nm. ULC deformability assessed using AFM showed that ULCs displayed a spread area of  $0.9 \pm 0.4 \mu\text{m}^2$  and a height of  $24.8 \pm 14.0$  nm (**Figure 1c**). CryoSEM analysis of ULC and activated platelet morphologies revealed that ULCs in suspension take on an activated platelet-like morphology, as marked by the protrusions and

particle-particle interactions present between the ULCs (**Figure 1d**). It is likely that the cryoSEM process is introducing deformation of the particles, and in the case of ULC particles this is pronounced and is likely the driving force between the observed interactions between polymers towards the outer edges of the particles. While this observation is likely a result of the cryoSEM process, it should be noted that previous studies using cryo-SEM imaging to characterize microgel morphology do not display this particle-particle interaction with more highly crosslinked (less deformable) particles and crosslinked microgels retain their spherical shape.<sup>17</sup> Overall, these results are indicative of the ability of the ULC particles to deform extensively and change shape, which is in contrast to crosslinked particles that do not exhibit this behavior.

*PLPs exert forces within and dynamically stiffen fibrin matrices*

After observing platelet-like morphologies and deformation behavior in unconjugated ULCs, ULCs were conjugated to fibrin-specific antibodies to create PLPs. Platelets are able to bind fibrin fibers within a polymerizing fibrin network and generate contractile forces within the network to induce clot retraction; since our PLPs contain fibrin-specific binding motifs and were shown to be capable of mimicking active platelet morphology and deformability, we hypothesized that PLPs would likewise be able to generate forces within a network to bring about clot contraction events and stiffen fibrin matrices. The ability of these PLPs to bring about platelet-mimetic clot retraction and changes in clot structure and mechanical properties was investigated using confocal microscopy, AFM, and micropost deflection (**Figure 2-4**). Native platelets generate forces within fibrin networks to cause collapses in clot microstructure and increase clot stiffness.<sup>37</sup> We hypothesized that conjugating fibrin-specific antibodies to deformable ULCs would likewise result in PLPs capable of generating forces within fibrin

networks to bring about collapses in clot structure and increases in clot stiffness. Confocal microscopy revealed that clots containing ULCs and control fibrin clots displayed less dense networks relative to clots containing PLPs (**Figure 2**). Analysis of clot structure was also performed using cryoSEM, which corroborated the trends seen in the confocal microscopy images (**Figure S2**). AFM was used to determine changes in clot elastic moduli in the presence of PLPs. Elastic moduli were found to increase significantly in the presence of PLPs, stiffening from  $1.21 \pm 0.50$  kPa 0 hours after polymerization to  $2.47 \pm 0.51$  kPa 24 hours after polymerization, relative to controls. Elastic moduli of control fibrin clots stiffened from  $0.79 \pm 0.15$  kPa 0 hours after polymerization to  $1.62 \pm 0.11$  kPa 24 hours after polymerization, and elastic moduli of fibrin clots containing unconjugated ULCs decreased slightly from  $0.19 \pm 0.10$  kPa 0 hours after polymerization to  $0.15 \pm 0.06$  kPa 24 hours after polymerization (**Figure 3**). These values for fibrin clots obtained 0 hours after polymerization and for PLP-incorporated clots obtained after 24 hours are consistent with those seen in the literature for unmodified fibrin clots ( $\sim 400$ - $800$  Pa) and retracted clots ( $\sim 3$  kPa), respectively.<sup>26, 38, 39</sup> The decreased clot modulus observed in the presence of the unmodified ULCs compared to control clots could be due to a slight inhibition of fibrin polymerization due to steric hindrance coupled with charge effects due to the non-binding particles. Micropost deflection revealed that force generation in PLP-incorporated clots was significantly greater than within ULC-incorporated clots or control fibrin clots (**Figure 4 a-e**); forces generated in PLP-incorporated clots were  $274 \pm 231$   $\mu$ N, whereas forces generated within ULC-incorporated clots and control fibrin clots were  $-128 \pm 503$   $\mu$ N and  $-67.5 \pm 140$   $\mu$ N, respectively. These negative force values likely indicate that the initial polymerization caused the clots to slightly contract around the microposts, and subsequent matrix relaxation caused less post deflection than was initially present due to

polymerization. This likely resulted in a negative direction of deflection and subsequent negative calculated force values.

Approximate calculations of the forces generated by a single PLP, obtained by dividing overall force generation by the number of PLPs contained within each fibrin clot surrounding the posts, revealed that an individual PLP generates a force of approximately  $6.5 \pm 5.5$  pN within the fibrin network. This is significantly lower than the forces generated by native active platelets, which have previously been reported as exhibiting average maximum contractile forces between 1.5 and 79 nN;<sup>37</sup> however, even at lower levels, this force generation brings about an overall significant increase in force generation within these networks relative to controls.

#### *PLPs enhance cell migration in an in vitro model of early wound healing*

Due to our results indicating that PLPs are capable of generating forces within fibrin matrices in order to increase matrix stiffness and the results of several previous studies indicating that increasing matrix stiffness brings about an increase in cell migration,<sup>7, 8</sup> we hypothesized that PLPs could be applied to fibrin matrices *in vitro* to increase cell migration within *in vitro* models of wound healing. We investigated this by embedding fibroblast spheroids within three-dimensional fibrin clot matrices and quantifying migration throughout the matrix (away from the spheroid bodies) over a period of 72 hours.<sup>29</sup> Quantification of fibroblast migration away from spheroid bodies embedded within control fibrin matrices or fibrin matrices containing either PLPs or ULCs revealed that cell migration through the matrix increased significantly in the presence of an optimal concentration of 0.5 mg/ml PLPs (**Figure 5**). Very little migration was observed from spheroids incorporated within fibrin matrices containing ULCs; we investigated whether this limited migration was due to charge effects created by the unconjugated particles by repeating the assay using uncharged ULCs (**Figure S3**), and found similar trends in migration

under these conditions as those observed in the presence of charged ULCs, indicating that charge effects are not the primary reason for the low degree of fibroblast migration seen in the fibrin + ULC matrices. It is likely that the softness of these matrices (1 kPa or less, as determined via AFM), decreased matrix density, and increased matrix porosity is a driver of this response.

*PLPs influence wound healing outcomes in a murine model of dermal injury*

There is indication that native platelets enhance wound healing *in vivo* through clot retraction and by enhancing reperfusion of blood to the tissues;<sup>3, 37</sup> furthermore, our findings from applying PLPs to *in vitro* models of fibroblast migration suggest that clot contraction enhances fibroblast migration within the fibrin matrix. During native wound healing, fibroblasts migrate into the wound environment, proliferate, and synthesize collagen. The provisional fibrin matrix is eventually degraded and replaced by this collagen, resulting in the formation of new tissue. Given the results shown previously indicating that PLPs are capable of bringing about clot retraction and subsequently enhancing fibroblast migration, we hypothesized that PLPs could be applied *in vivo* to enhance wound closure rates and improve healing. We investigated this by topically applying PLPs (0.5, 1.0, and 2.0 mg/ml concentrations) or saline in a murine model of full thickness dermal injury. We postulated that there would be sufficient native fibrin formation with which the PLPs could bind and interact. We performed immunohistochemistry on tissue sections harvested 9 days post-injury to determine colocalization of PLPs and fibrin throughout the wound area (**Figure S4**). These studies demonstrate robust colocalization of PLPs with fibrin in the wound bed. It appears that the PLPs are also interacting extensively with fibrin polymers; however, the resolution of the histological sections would need to be enhanced in order to definitively make this claim. Analysis of wound closure over 9 days indicated a dose-dependent response in which increased concentrations of topically applied PLPs improve rates of wound

closure (**Figure 6**). Histological evaluation of tissues collected 9 days post-injury and stained with Martius Scarlet Blue (MSB) revealed more robust epithelial layer formation in tissues treated with 1 mg/ml PLPs relative to tissues treated with saline ( $p < 0.0001$ ), 0.5 mg/ml PLPs ( $p < 0.05$ ), or 2.0 mg/ml PLPs ( $p < 0.0001$ ) (**Figure 7a-b**). IHC labeling for angiogenesis marker CD31 showed increased angiogenesis in tissues treated with 1 mg/ml PLPs relative to tissues treated with saline, 0.5 mg/ml PLPs, and 2.0 mg/ml PLPs ( $p < 0.05$ ) (**Figure 7a,c**).

We also investigated the ability of PLPs to bring about wound healing when incorporated into fibrin polymers upon initial treatment. Histological evaluation of tissues collected 9 days post injury and stained with MSB and CD31 markers revealed significantly improved epidermal thickness and angiogenesis in wounds treated with PLPs incorporated into fibrin polymers relative to those treated with saline, control fibrin polymers, or fibrin polymers + ULC (**Figure 8 a-c**). We also evaluated a standard-of-care technology (platelet-rich plasma (PRP)) treatment group in order to compare the wound healing effects of PLPs with the wound healing effects of the PRP treatment. Wounds treated with PLP clots showed significantly increased angiogenesis in tissues collected 9 days post-injury relative to wounds treated with PRP; both conditions showed comparable levels of enhanced epidermal thickness relative to saline controls (**Figure 8**). Representative images of wounds and closure rates are presented in **Figure S5**. Hematoxylin and eosin (H&E) staining of wounds treated with fibrin + PLP polymers also show robust stratum spinosum formation relative to other treatment conditions, indicating improved epidermal regeneration relative to wounds treated with controls or PRP. Additionally, incorporation of ULCs into fibrin polymers resulted in a large degree of fibrosis, as seen in the MSB images of wounds treated with fibrin + ULC polymers, indicating that the fibrin-targeting ability of the PLPs is necessary to bring about improved healing rather than solely the

deformability of the base microgel particles. Epidermal thickness values observed in the PLP clots were similar to those observed in our initial studies in wounds treated topically with 1.0 mg/ml PLP. For these studies in which PLPs were incorporated into fibrin clots, we chose a concentration of 0.5 mg/ml PLPs, since that concentration had proved optimal for improving cell migration within a PLP-incorporated clot in our previous *in vitro* experiments. Collectively, these studies demonstrate that PLPs could be applied directly to a wound or within a fibrin clot, though it should be noted that angiogenesis was more extensive when the PLPs were applied within the fibrin network.

Statistically significant differences were not observed in the wound closure rates calculated for these studies, despite significant differences in the histological evaluation of wound tissues across groups. This is a limitation of this study and could have arisen due to the small area of the starting wounds and/or the small sample size of this study.

In these studies, we demonstrate that fibrin-binding PLPs constructed from highly deformable microgels are capable of mimicking activated platelet morphology, generating contractile forces within fibrin clots and inducing clot retraction, resulting in increased clot stiffness. Additionally, PLPs enhance cell migration *in vitro* and enhance healing outcomes *in vivo*. These studies demonstrate the utility of platelet mimetic materials beyond hemostatic applications and show that PLPs capable of inducing clot retraction can additionally improve subsequent healing responses.

Characterization of ULC microgels using nanoparticle tracking, AFM, and cryoSEM revealed that these ULCs are capable of contracting and spreading to high degrees, as marked by their hydrodynamic radii, spread diameter, and spread height. This indicates that these ULCs are capable of recapitulating a key mechanical function of native activated platelets: the ability to

deform within fibrin networks to bring about clot retraction. CryoSEM also indicated that these ULCs take on an active-platelet like morphology in suspension, as marked by the protrusions and particle-particle interactions present in the ULC suspensions. These results indicate that the minimal degree of crosslinking present in these particles allows them to mimic native platelet interactions and mechanics.

Evaluation of fibrin-binding PLPs and non-binding ULCs impact upon fibrin clots revealed that clots containing PLPs had significant increases in density, stiffness, and force generation relative to control fibrin clots, whereas clots containing ULCs generally showed lower density, stiffness, and force generation than control fibrin clots. It is likely that the decreased mechanical properties exhibited by ULC clots occurs as a result of steric hindrance during fibrin polymerization brought about by these particles embedded within the fibrin network. The significant increase in mechanical properties exhibited by the PLP clots relative to both the control and ULC clots indicates that this steric hindrance does not occur when the particles are coupled to a fibrin-specific antibody; the antibody allows the PLPs to interact with the fibrin fibers within the network rather than incorporate nonspecifically into the pores. This interaction allows the particles to generate forces within the network, pulling on the fibers to generate microcollapses in the network structure that lead to stiffer clots with decreased porosity and increased density; therefore, these results indicate that it is the combination of the unique deformability and the fibrin specificity of these PLPs that allows them to recapitulate native platelet-mediated clot retraction.

We also found that an optimal concentration of PLPs resulted in increased fibroblast migration in a three-dimensional model of migration through a provisional fibrin matrix. However, we also found that higher concentrations of PLPs seemed to inhibit rather than

enhance fibroblast migration; we suspect this may be due to steric hindrance of the clot contraction event brought about by an overload of particles within the fibrin network. Migration through ULC clot matrices decreased relative to migration through control fibrin matrices and PLP clot matrices, further indicating that the stiffness of the provisional fibrin matrix plays a role in the degree of fibroblast migration and suggesting that the increased matrix stiffness induced by PLPs at an optimized concentration can facilitate enhanced degrees of fibroblast migration throughout a provisional fibrin matrix, such as those present in the early stages of wound healing.

Topical application of PLPs *in vivo* revealed a dose-dependent increase in wound closure rate with increasing concentration of PLPs, ranging from 0.5 – 2.0 mg/ml. Healing at 1.0 mg/ml showed improved epithelial layer formation and more robust angiogenesis than in other conditions; while this is higher than the optimal concentration found previously for *in vitro* studies, inherent differences in *in vitro* and *in vivo* systems often result in variations in optimal treatment dose concentrations. IHC stains of wound cross-sections revealed greater angiogenesis in tissues treated with optimal concentrations of PLPs and decreased angiogenesis in tissues treated with concentrations higher than the optimal 1.0 mg/ml concentration, mirroring the impaired cellular migration responses seen *in vitro* at PLP concentrations higher than the optimal *in vitro* concentration of 0.5 mg/ml. These results indicate that topical application of PLPs to a murine full thickness dermal injury model improves overall wound healing outcomes.

Application of PLPs within a fibrin polymer *in vivo* likewise revealed improved healing outcomes in wounds treated with fibrin polymers containing PLPs relative to other conditions. IHC stains of wound cross-sections revealed greater angiogenesis in tissues treated with fibrin + PLP polymers compared to control polymers or PRP. MSB and H&E stains of wound cross-

sections revealed enhanced epidermal thickness and more robust stratum spinosum formation in wounds treated with fibrin + PLP polymers relative to other conditions, indicating improved epidermal regeneration within these tissues. These results indicate that application of PLPs within a fibrin matrix to a murine full thickness dermal injury model likewise improves wound healing outcomes.

## Conclusions

Overall, these studies show that synthetic particles that mimic platelet morphology are capable of generating forces within and dynamically stiffening clots, promoting cell migration, and enhancing wound healing, indicating that they act in a manner similar to micromachines such as actin-myosin molecular motors. While several synthetic platelet technologies have been previously developed, most are primarily focused on participation in primary hemostasis;<sup>1, 14, 40-44</sup> a unique aspect of our PLPs is their ability to participate in secondary hemostasis and, through force generation and dynamic stiffening of fibrin networks, promote clot retraction. Furthermore, although it has been understood that activated platelets interact with fibrin polymerizing at wound sites to form a hemostatic “plug” during primary hemostasis, the role of native platelet-mediated clot retraction in wound healing has not been well understood. The results found in these studies contribute to our understanding of native platelet biology, particularly within the context of clot contraction, and indicate that platelet-induced clot contraction plays a large role in promoting fibroblast migration into the provisional matrix and subsequently promoting overall tissue repair.

Application of ULC pNIPAm PLPs to fibrin clots and to *in vitro* and *in vivo* models of wound healing indicates that PLPs are capable of generating forces within fibrin networks in order to mechanically mediate cell migration and wound healing outcomes. Native platelets exert

contractile forces upon fibrin fibers to stabilize bleeding and stiffen fibrin matrices to facilitate subsequent stages of wound healing. The ability to mimic this platelet-fibrin interaction via deformable PLPs that can exert strain upon fibrin fibers provides a biomimetic platform that could be applied to multiple stages of wound healing. The clot contraction abilities of these PLPs could be applied to models of uncontrolled bleeding to improve hemostatic responses in traumatic injury or disease models, and the ability to apply PLPs to fibrin or other fibrillar matrices to tune matrix mechanical properties could be used to enhance healing beyond initial hemostasis.

**Conflicts of interest:** The authors have no conflicts of interest to declare.

**Acknowledgements:** Funding for this project was provided by the American Heart Association (16SDG29870005) and the National Institutes of Health NIAMS (R21AR071017). This work was performed in part at the North Carolina State University Analytical Instrumentation Facility (AIF), which is supported by the State of North Carolina and the National Science Foundation (ECCS-1542015). The AIF is part of the North Carolina Research Triangle Nanotechnology Network (RTNN), a site in the National Nanotechnology Coordinated Infrastructure (NNCI). The authors acknowledge M. Castaneda and S. Funderburk for assistance with ULC synthesis, D. Chester for assistance with AFM, P. Erb for micropost mold fabrication, S. Ambati for assistance with micropost fabrication, E. Mihalko for assistance with PRP isolation, and C. Zhou at the AIF for assistance with cryoSEM.

## Figures

Figure 1

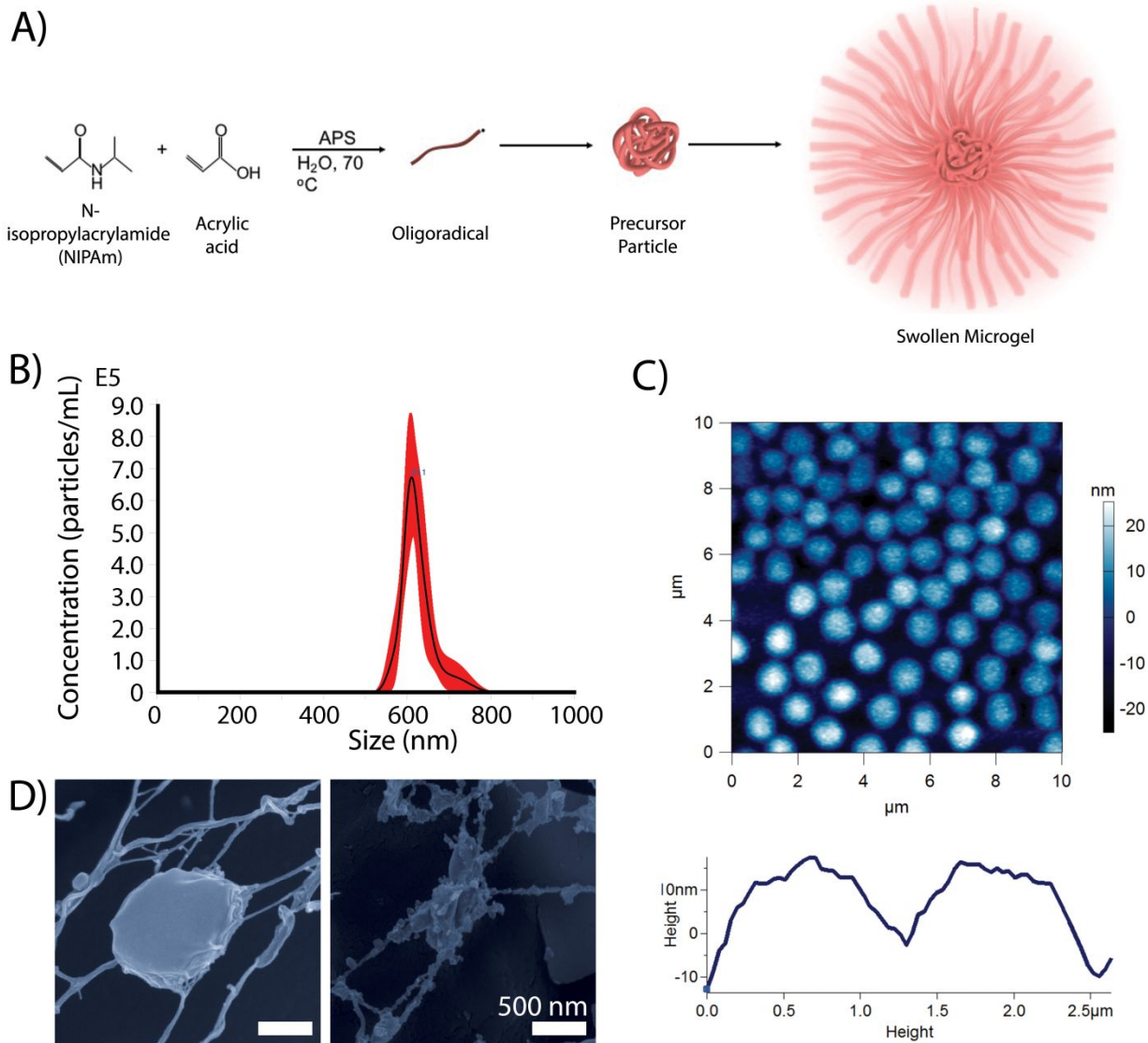


Figure 2

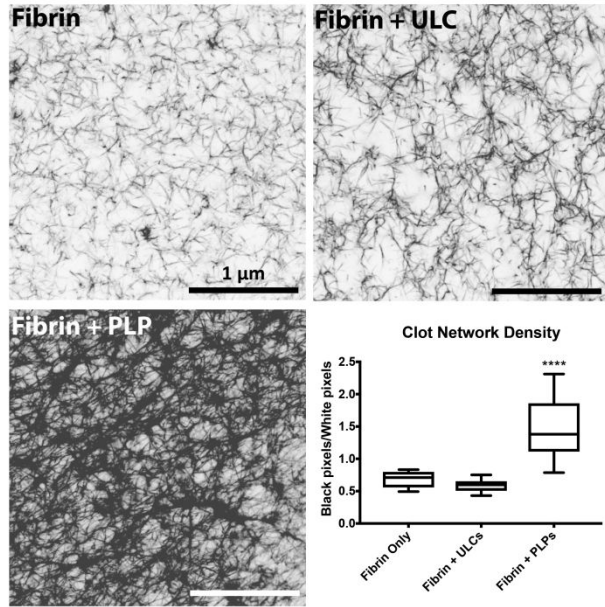


Figure 3

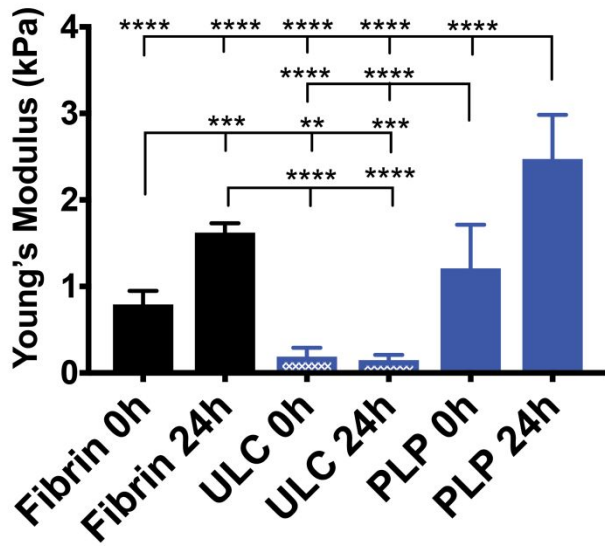
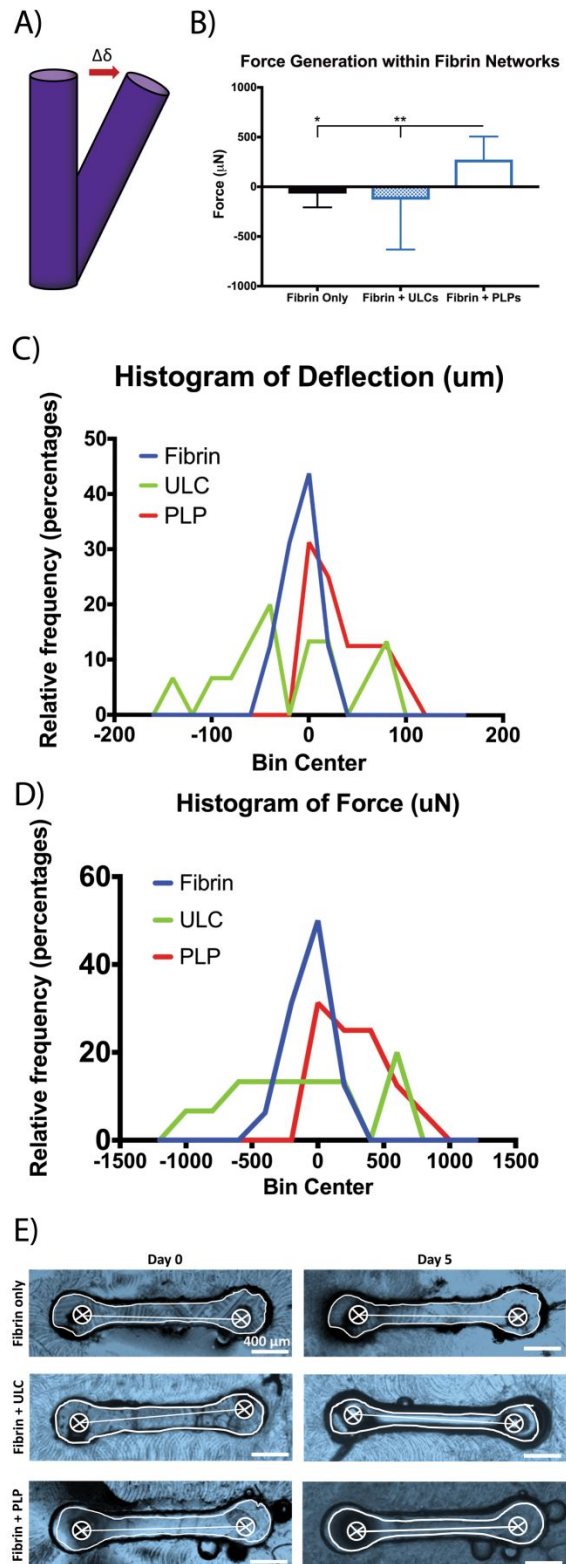
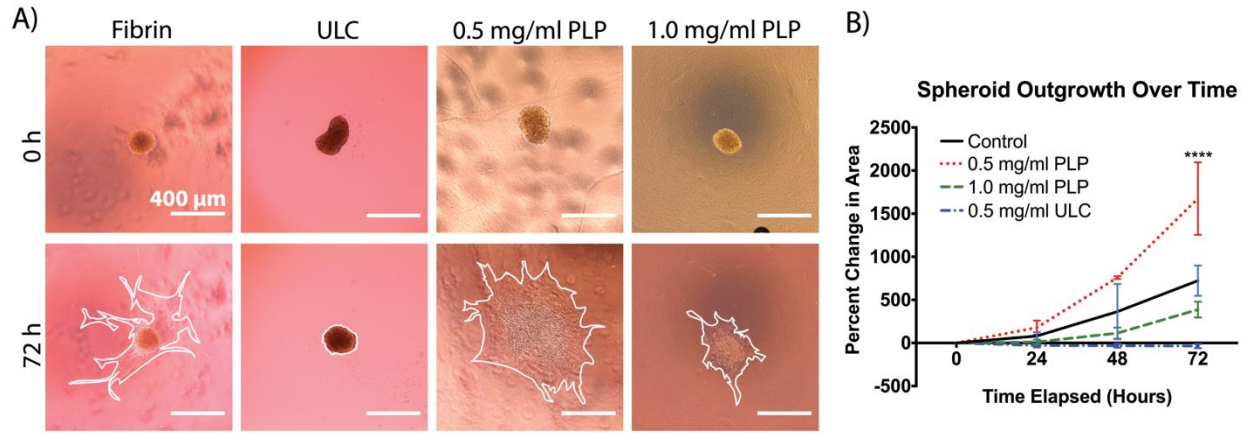


Figure 4



**Figure 5**



**Figure 6**

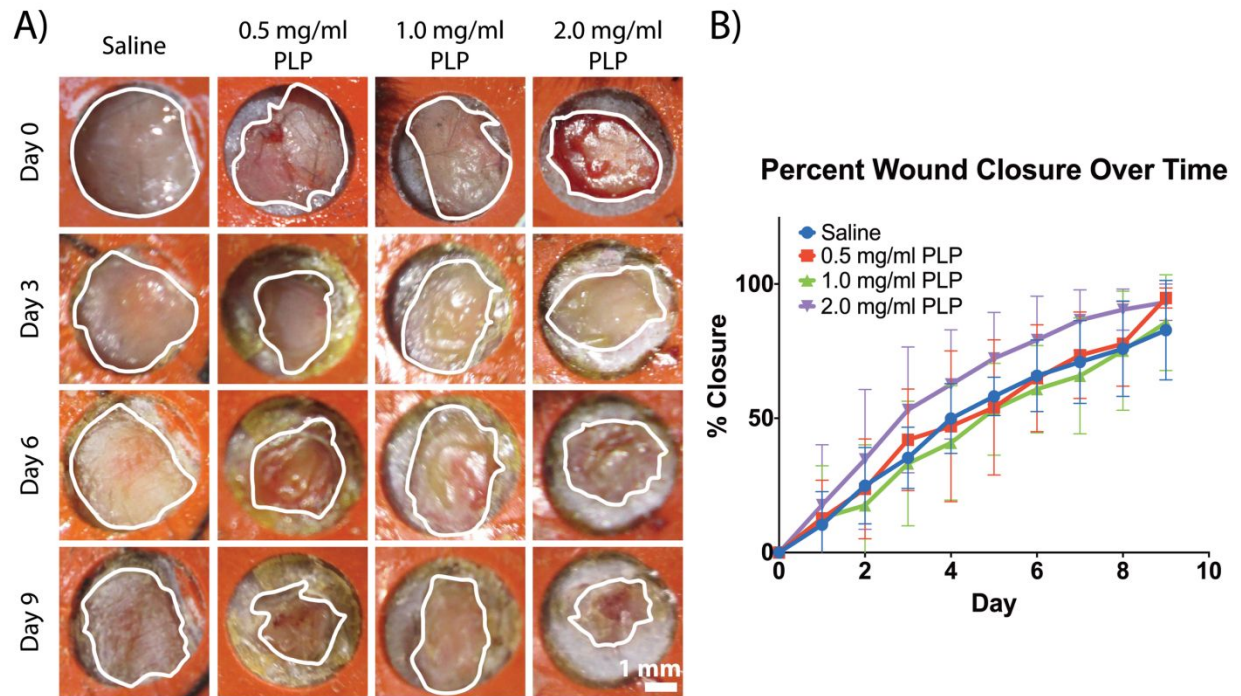


Figure 7

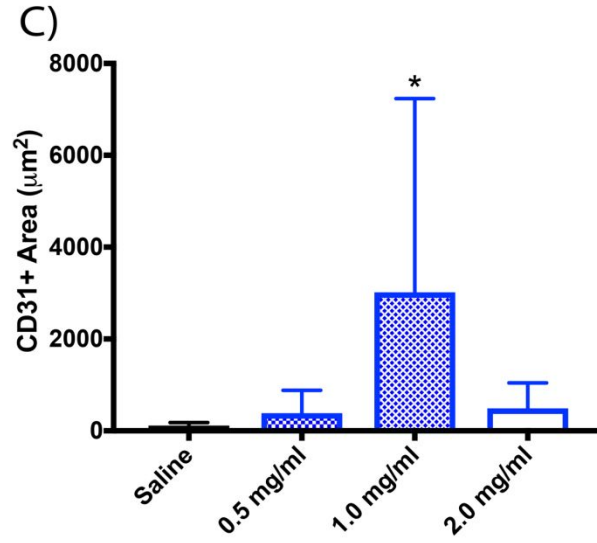
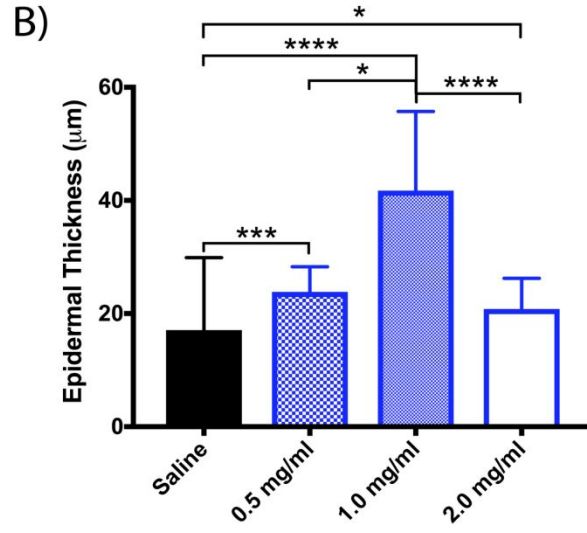
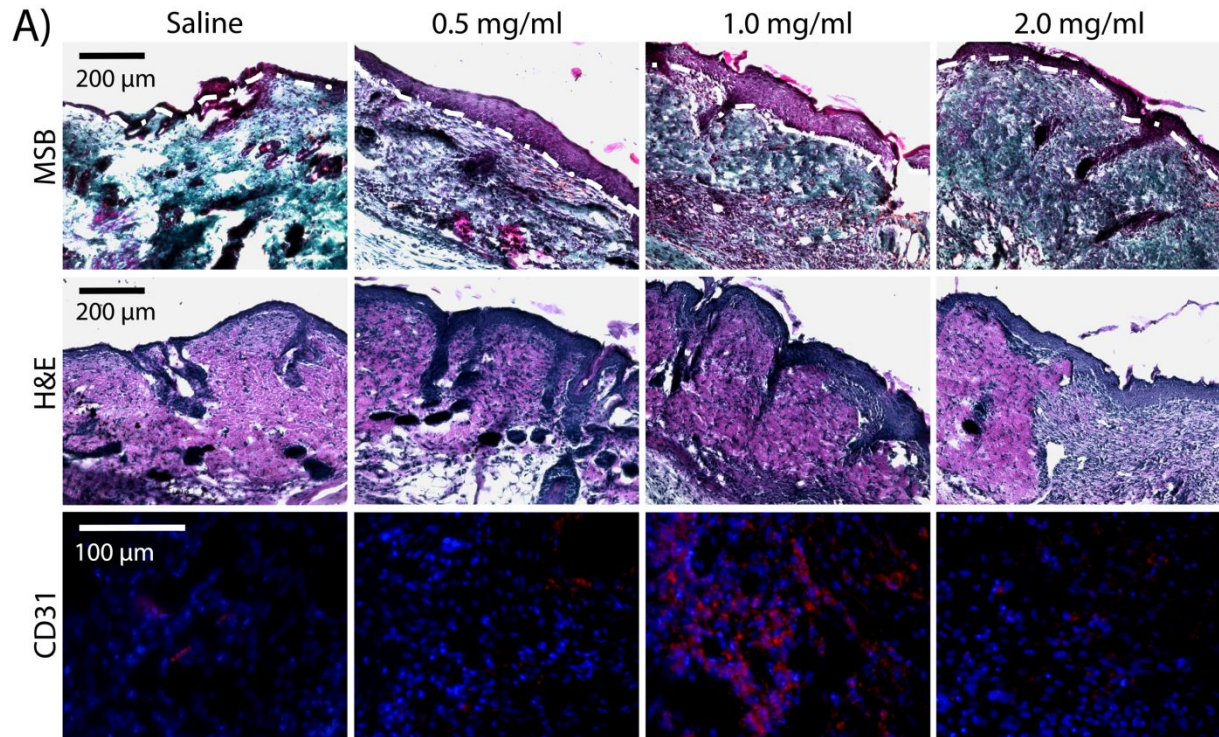
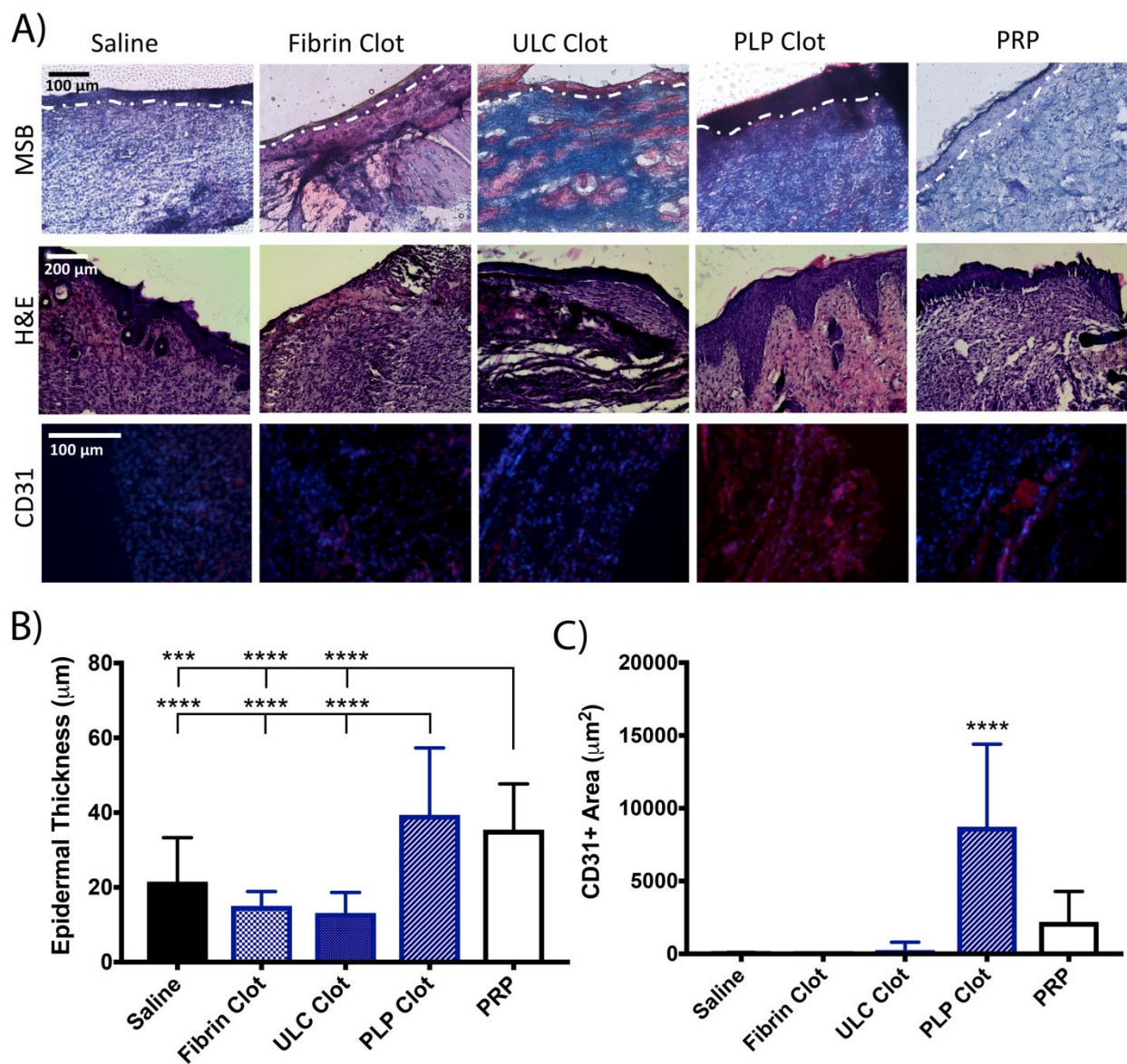


Figure 8



**Figure 1:** Microgel characterization. A) pNIPAm-*co*-AAc ULCs are synthesized via a precipitation polymerization reaction. B) ULCs in their collapsed state have a hydrodynamic radius of  $624 \pm 32$  nm with a Gaussian size distribution. C) AFM dry imaging of ULCs show that ULC particles deform to have low heights and diameters of  $\sim 1$  micron. D) CryoSEM imaging of ULCs in suspension reveal that ULCs take on an activated platelet-like morphology, mimicking spindle-like protrusions and particle-particle interactions.

**Figure 2:** Confocal microscopy of fibrin clots taken at 63X magnification reveal that clots containing PLPs are significantly denser than control clots or clots containing ULCs, as determined by calculating black pixel area (fibrin fibers) over white pixel area (negative space). n = 3 clots/group, 3 images/clot; \*\*\*\*:  $p < 0.0001$

**Figure 3:** PLPs dynamically stiffen fibrin matrices. Clots were allowed to polymerize for 1 hour prior to acquiring Young's modulus values using AFM force mapping. Young's moduli of fibrin clots obtained 0 and 24 hours after the polymerization period reveal that incorporation of PLPs in clots result in a significant increase in clot elastic modulus, whereas incorporation of ULCs into clots decreases stiffness. Average Young's modulus  $\pm$  standard deviation are presented in the graph; n = 3 clots/group, 3 force maps/clot, 256 force curves/force map; \*\*:  $p < 0.01$ ; \*\*\*\*:  $p < 0.0001$

**Figure 4:** Force generation within fibrin networks. A) Schematic of PDMS post deflection. As forces are generated within fibrin networks, PDMS posts are deflected; force generation can be calculated based on the deflection of the posts. B) PLP-incorporated clots generate significantly higher forces within fibrin networks than control fibrin clots and ULC-incorporated clots. C, D) Histograms of post deflection and associated force generation. The histograms of deflection and associated force generation is skewed towards the right for clots incorporated with PLPs, indicating trend of increased forces within these networks relative to controls. E) PLP-incorporated fibrin clots contract around the PDMS posts to deflect post beams. Representative bright field top-view images of microposts and clots at days 0 and 5 are shown. Post centers were determined based on the known diameters of the posts; centers were determined using two diameters for each post, after which center-to-center distance could be determined. n = 16/group; \*:  $p < 0.05$ ; \*\*:  $p < 0.01$ .

**Figure 5:** A) Fibroblast migration throughout the clot matrix is quantified using ImageJ by tracing the cell body boundary. Outlines of the cell boundary after 72 hours are shown in white. B) Fibroblast migration significantly increases in the presence of an optimized concentration of PLPs. Mean percent change in spheroid area is presented  $\pm$  standard deviation.  $n = 6/\text{group}$ ; \*\*\*\*:  $p < 0.0001$

**Figure 6:** PLPs enhance wound healing *in vivo*. A murine full-thickness dermal injury model was used to investigate dermal healing following topical application of PLPs (0, 0.5, 1.0, or 2.0 mg/ml dosages). Representative wound images over time are shown (A); outlines of the wound boundaries are shown in white. B) Percent wound closure was calculated; mean percent closure  $\pm$  standard deviation are presented.  $n = 5$  wounds/group.

**Figure 7:** A) Martius Scarlet Blue (MSB) and hematoxylin and eosin (H&E) staining of wounds harvested 9 days post-injury reveals more robust healing and epidermal layer formation in wounds treated with a dosage of 1 mg/ml PLPs. Immunohistochemical analysis of wounds collected 9 days post-injury shows greater CD31+ tissue in wounds treated with 1 mg/ml PLPs. Epidermal thickness, presented in (B), was quantified using MSB images. Mean epidermal thickness  $\pm$  standard deviation is shown. C) Immunohistochemical analysis of wounds collected 9 days post-injury shows increased CD31+ areas (red) in wounds treated with 1 mg/ml PLPs. Mean CD31+ area  $\pm$  standard deviation is shown.  $n = 5$  wounds/group; \*:  $p < 0.05$ ; \*\*:  $p < 0.01$ ; \*\*\*:  $p < 0.001$ ; \*\*\*\*:  $p < 0.0001$ .

**Figure 8:** A) H&E and Martius Scarlet Blue (MSB) staining of wounds harvested 9 days post-injury reveals more robust healing and epidermal layer formation in wounds treated with fibrin polymers containing PLPs relative to controls. MSB images were used to quantify epidermal thickness in (B); the outline of the epidermis on the MSB images is shown in white.

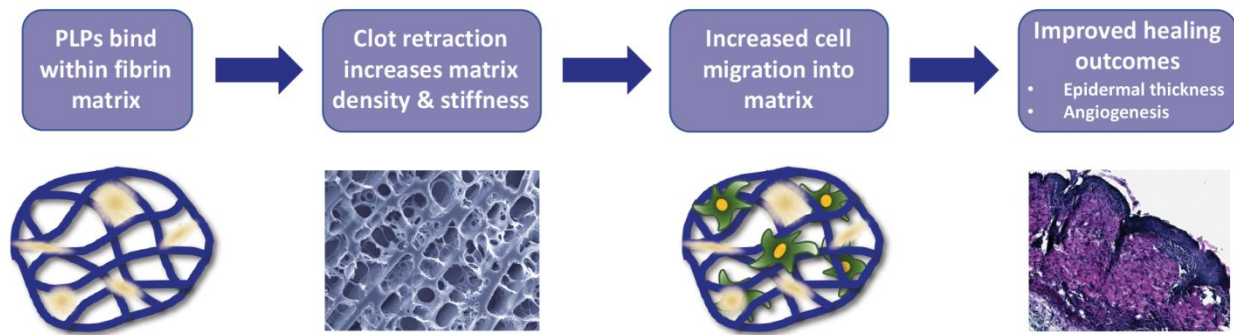
Immunohistochemical analysis of wounds collected 9 days post-injury shows greater CD31+ tissue in wounds treated with fibrin polymers containing PLPs. B) Epidermal thickness, evaluated using MSB images, is significantly increased in wounds treated with fibrin polymers containing PLPs. Mean epidermal thickness  $\pm$  standard deviation is shown. C) Immunohistochemical analysis of wounds collected 9 days post-injury shows increased CD31+ areas (red) in wounds treated with fibrin polymers containing PLPs. Mean CD31+ area  $\pm$  standard deviation is shown. n = 5 wounds/group; \*\*\*: p < 0.001; \*\*\*\*: p < 0.0001.

### References:

1. C. L. Modery-Pawlowski, L. L. Tian, V. Pan, K. R. McCrae, S. Mitragotri and A. Sen Gupta, *Biomaterials*, 2013, **34**, 526-541.
2. J. W. Yau, H. Teoh and S. Verma, *BMC Cardiovascular Disorders*, 2015, **15**.
3. D. B. Cines, T. Lebedeva, C. Nagaswami, V. Hayes, W. Masefski, R. I. Litvinov, L. Rauova, T. J. Lowery and J. W. Weisel, *Blood*, 2014, **123**, 1596-1603.
4. O. V. Kim, R. I. Litvinov, M. S. Alber and J. W. Weisel, *Nat Commun*, 2017, **8**, 1274.
5. J. W. Weisel and R. I. Litvinov, *Blood*, 2013, **121**, 1712-1719.
6. L. E. Dickinson and S. Gerecht, *Frontiers in Physiology*, 2016, **7**.
7. J. R. Tse and A. J. Engler, *PLOS ONE*, 2011, **6**, e15978.
8. A. J. Engler, S. Sen, H. L. Sweeney and D. E. Discher, *Cell*, **126**, 677-689.
9. A. Chabert, H. Hamzeh-Cognasse, B. Pozzetto, F. Cognasse, M. Schattner, R. M. Gomez and O. Garraud, *BMC Immunology*, 2015, **16**.
10. J. A. Evans, K. J. P. van Wessem, D. McDougall, K. A. Lee, T. Lyons and Z. J. Balogh, *World Journal of Surgery*, 2010, **34**, 158-163.
11. H. Wandt, K. Schaefer-Eckart, K. Wendelin, B. Pilz, M. Wilhelm, M. Thalheimer, U. Mahlke, A. Ho, M. Schaich, M. Kramer and others, *The Lancet*, 2012, **380**, 1309-1316.
12. S. J. Stanworth, L. J. Estcourt, G. Powter, B. C. Kahan, C. Dyer, L. Choo, L. Bakrania, C. Llewelyn, T. Littlewood, R. Soutar, D. Norfolk, A. Coppstone, N. Smith, P. Kerr, G. Jones, K. Raj, D. A. Westerman, J. Szer, N. Jackson, P. G. Bardy, D. Plews, S. Lyons, L. Bielby, E. M. Wood and M. F. Murphy, *New England Journal of Medicine*, 2013, **368**, 1771-1780.
13. S. Nandi and A. C. Brown, *Exp Biol Med (Maywood)*, 2016, **241**, 1138-1148.
14. C. L. Modery-Pawlowski, L. L. Tian, M. Ravikumar, T. L. Wong and A. S. Gupta, *Biomaterials*, 2013, **34**, 3031-3041.
15. A. C. Brown, S. E. Stabenfeldt, B. Ahn, R. T. Hannan, K. S. Dhada, E. S. Herman, V. Stefanelli, N. Guzzetta, A. Alexeev, W. A. Lam, L. A. Lyon and T. H. Barker, *Nature Materials*, 2014, **13**, 1108-1114.
16. E. P. Sproul, S. Nandi, C. Roosa, L. Schreck and A. C. Brown, *Advanced Biosystems*, 2018, **0**, 1800042.

17. A. Joshi, S. Nandi, D. Chester, A. C. Brown and M. Muller, *Langmuir*, 2017, DOI: 10.1021/acs.langmuir.7b02801.
18. H. Bachman, A. C. Brown, K. C. Clarke, K. S. Dhada, A. Douglas, C. E. Hansen, E. Herman, J. S. Hyatt, P. Kodlekere, Z. Meng, S. Saxena, M. W. Spears Jr, N. Welsch and L. A. Lyon, *Soft Matter*, 2015, **11**, 2018-2028.
19. J.-P. Cazenave, P. Ohlmann, D. Cassel, A. Eckly, B. Hechler and C. Gachet, in *Platelets and Megakaryocytes*, 2004, vol. 272, pp. 13-28.
20. K. M. Beussman, M. L. Rodriguez, A. Leonard, N. Taparia, C. R. Thompson and N. J. Sniadecki, *Methods (San Diego, Calif.)*, 2016, **94**, 43-50.
21. N. Goedecke, M. Bollhalder, R. Bernet, U. Silvan and J. Snedeker, *J Vis Exp*, 2015, DOI: 10.3791/53350, 53350.
22. M. L. Rodriguez, B. T. Graham, L. M. Pabon, S. J. Han, C. E. Murry and N. J. Sniadecki, *Journal of Biomechanical Engineering*, 2014, **136**, 0510051-05100510.
23. N. Thavandiran, N. Dubois, A. Mikryukov, S. Massé, B. Beca, C. A. Simmons, V. S. Deshpande, J. P. McGarry, C. S. Chen, K. Nanthakumar, G. M. Keller, M. Radisic and P. W. Zandstra, *Proceedings of the National Academy of Sciences of the United States of America*, 2013, **110**, E4698-E4707.
24. A. Hansen, A. Eder, M. Bonstrup, M. Flato, M. Mewe, S. Schaaf, B. Aksehrlioglu, A. Schwoerer, J. Uebeler and T. Eschenhagen, *Circulation Research*, 2010, **107**, 35-44.
25. H. Vandenburg, *Tissue Eng Part B Rev*, 2010, **16**, 55-64.
26. N. Welsch and L. A. Lyon, *PLOS ONE*, 2017, **12**, e0181369-e0181369.
27. J. J. Roa, G. Oncins, J. Diaz, F. Sanz and M. Segarra, *Recent Patents on Nanotechnology*, 2011, **5**, 27-36.
28. A. Vinckier and G. Semenza, *FEBS Letters*, 1998, **430**, 12-16.
29. S. Nandi and A. C. Brown, 2017, DOI: doi:10.3791/56099, e56099.
30. J. W. Weisel, in *Advances in Protein Chemistry*, Academic Press, 2005, vol. 70, pp. 247-299.
31. V. K. Lishko, T. Burke and T. Ugarova, *Blood*, 2007, **109**, 1541-1549.
32. R. A. S. Ariëns, *Journal of Thrombosis and Haemostasis*, 2013, **11**, 294-305.
33. L. Dunn, H. C. G. Prosser, J. T. M. Tan, L. Z. Vanags, M. K. C. Ng and C. A. Bursill, *J Vis Exp*, 2013, DOI: 10.3791/50265, 50265.
34. Y. Menchisheva, U. Mirzakulova and R. Yui, *International Wound Journal*, 2018, **0**.
35. E. B. Cho, G. S. Park, S. S. Park, Y. J. Jang, K. H. Kim, K. J. Kim and E. J. Park, *Journal of Cosmetic Dermatology*, 2018, **0**.
36. O. H. Alser and I. Goutos, *Scars, burns & healing*, 2018, **4**, 2059513118808773-2059513118808773.
37. W. A. Lam, O. Chaudhuri, A. Crow, K. D. Webster, T.-D. Li, A. Kita, J. Huang and D. A. Fletcher, *Nature Materials*, 2011, **10**, 61-66.
38. K. P. Mercado-Shekhar, R. Kleven, H. Aponte Rivera, R. Lewis, K. B. Karani, H. J. Vos, T. A. Abruzzo, K. J. Haworth and C. K. Holland, *The Journal of the Acoustical Society of America*, 2018, **143**, 1928-1928.
39. J. P. Winer, S. Oake and P. A. Janmey, *PLOS ONE*, 2009, **4**, e6382.
40. A. C. Anselmo, C. L. Modery-Pawlowski, S. Menegatti, S. Kumar, D. R. Vogus, L. L. Tian, M. Chen, T. M. Squires, A. Sen Gupta and S. Mitragotri, *ACS Nano*, 2014, **8**, 11243-11253.

41. H. Haji-Valizadeh, C. L. Modery-Pawłowski and A. Sen Gupta, *Nanoscale*, 2014, **6**, 4765.
42. M. Ravikumar, C. L. Modery, T. L. Wong, M. Dzuricky and A. Sen Gupta, *Bioconjugate Chemistry*, 2012, **23**, 1266-1275.
43. M. Ravikumar, C. L. Modery, T. L. Wong and A. Sen Gupta, *Biomacromolecules*, 2012, **13**, 1495-1502.
44. N. Doshi, J. N. Orje, B. Molins, J. W. Smith, S. Mitragotri and Z. M. Ruggeri, *Advanced Materials*, 2012, **24**, 3864-3869.

**TOC Figure**

PLPs increase fibrin stiffness, promote cell migration, and improve healing outcomes.